Journal of Applied Physics

Electric-field-controlled interface strain coupling and non-volatile resistance switching of $La_{1-x}Ba_xMnO_3$ thin films epitaxially grown on relaxor-based ferroelectric single crystals

Cite as: J. Appl. Phys. **116**, 113911 (2014); https://doi.org/10.1063/1.4896172
Submitted: 10 July 2014 . Accepted: 09 September 2014 . Published Online: 19 September 2014

Ming Zheng, Qiu-Xiang Zhu, Xue-Yan Li, Ming-Min Yang, Yu Wang, Xiao-Min Li, Xun Shi, Hao-Su Luo, and Ren-Kui Zheng

AIP Publishing

Electric-field-controlled interface strain coupling and non-volatile resistance switching of $La_{1-x}Ba_xMnO_3$ thin films epitaxially grown on relaxor-based ferroelectric single crystals

Ming Zheng,[1] Qiu-Xiang Zhu,[1] Xue-Yan Li,[1] Ming-Min Yang,[1] Yu Wang,[2] Xiao-Min Li,[1] Xun Shi,[1] Hao-Su Luo,[1] and Ren-Kui Zheng[1,a)]
[1]*State Key Laboratory of High Performance Ceramics and Superfine Microstructure, Shanghai Institute of Ceramics, Chinese Academy of Sciences, Shanghai 200050, China*
[2]*Department of Applied Physics, The Hong Kong Polytechnic University, Hong Kong, China*

(Received 10 July 2014; accepted 9 September 2014; published online 19 September 2014)

We have fabricated magnetoelectric heterostructures by growing ferromagnetic $La_{1-x}Ba_xMnO_3$ ($x = 0.2$, 0.4) thin films on (001)-, (110)-, and (111)-oriented $0.31Pb(In_{1/2}Nb_{1/2})O_3$-$0.35Pb(Mg_{1/3}Nb_{1/2})O_3$-$0.34PbTiO_3$ (PINT) ferroelectric single-crystal substrates. Upon poling along the [001], [110], or [111] crystal direction, the electric-field-induced non-180° domain switching gives rise to a decrease in the resistance and an enhancement of the metal-to-insulator transition temperature T_C of the films. By taking advantage of the 180° ferroelectric domain switching, we identify that such changes in the resistance and T_C are caused by domain switching-induced strain but not domain switching-induced accumulation or depletion of charge carriers at the interface. Further, we found that the domain switching-induced strain effects can be efficiently controlled by a magnetic field, mediated by the electronic phase separation. Moreover, we determined the evolution of the strength of the electronic phase separation against temperature and magnetic field by recording the strain-tunability of the resistance $[(\Delta R/R)_{strain}]$ under magnetic fields. Additionally, opposing effects of domain switching-induced strain on ferromagnetism above and below 197 K for the $La_{0.8}Ba_{0.2}MnO_3$ film and 150 K for the $La_{0.6}Ba_{0.4}MnO_3$ film, respectively, were observed and explained by the magnetoelastic effect through adjusting the magnetic anisotropy. Finally, using the reversible ferroelastic domain switching of the PINT, we realized non-volatile resistance switching of the films at room temperature, implying potential applications of the magnetoelectric heterostructure in non-volatile memory devices. © *2014 AIP Publishing LLC*.
[http://dx.doi.org/10.1063/1.4896172]

I. INTRODUCTION

Multiferroic heterostructures composed of ferromagnetic thin-film layer and ferroelectric (FE) polycrystalline or single-crystal layer have sparked a surge of research activities due to the strong strain- and/or charge-mediated converse magnetoelectric (ME) coupling effect, which can be readily realized by the application of an electric field (E) across the FE layer.[1–15] Apart from the well studied strain-mediated converse ME coupling,[1–10] electric-field-induced interfacial electric charge has been used to achieve a strong ME coupling between the magnetic and the electric order parameters.[11–14] Combining both the strain and electric charge, Nan *et al.*[15] achieved a significantly enhanced converse magnetoelectric coupling in the ultra-thin $Ni_{0.79}Fe_{0.21}$ film/$0.71Pb(Mg_{1/3}Nb_{1/2})O_3$-$0.29PbTiO_3$ single crystal multiferroic heterostructures. Perovskite manganites of $La_{1-x}Ba_xMnO_3$ possess various attractive physical phenomena, such as the colossal magnetoresistance (CMR) effect, the metal-to-insulator transition, and the electronic phase separation (EPS) [i.e., the coexistence of the ferromagnetic metallic phase (FMM) and the charge-ordered antiferromagnetic insulating phase],[16] which are sensitive to charge carrier concentration and lattice strain due to the strong interplay among the spin, charge, lattice, and orbital degrees of freedom. For example, Kanki *et al.*[17] achieved 2.5 K reversible shift in the metal-to-insulator transition temperature by electric-field control of accumulation/depletion of charge carriers at the interface for the $La_{0.85}Ba_{0.15}MnO_3/Pb(Zr_{0.2}Ti_{0.8})O_3$ heterostructure. Li and Zhu *et al.*[18,19] reported electric-field control of resistance and magnetization of $La_{1-x}Ba_xMnO_3$ films grown on FE single-crystal substrates, through ferroelectric poling of FE substrates. However, such electric-field induced poling of FE substrates is irreversible, resulting in irreversible changes in the lattice strain and physical properties of the films. Recently, non-volatile and reversible physical property modulation has been achieved for several thin films ($Bi_{0.95}Mn_{0.05}FeO_3$,[20] Fe_3O_4,[21] VO_2,[22] $Co_{40}Fe_{40}B_{20}$ (Ref. 23)) grown on FE single-crystal substrates [e.g., $(1-x)Pb(Mg_{1/3}Nb_{1/2})O_3$-$xPbTiO_3$ (PMN-PT)] in which two stable and reversible remnant strain states could be induced via the non-180° ferroelastic domain switching.[10,20–23] Despite much effort has been devoted to the non-volatile switching of physical parameters of several oxide and non-oxide thin films, the ferroelectric domain switching-induced strain on physical properties of perovskite manganite films (e.g., $La_{1-x}Ba_xMnO_3$) is still poorly understood. Moreover, certain important issues concerning the $La_{1-x}Ba_xMnO_3$ films still remain unclear, for example, whether the in-plane compressive strain enhances or suppresses the

a)E-mail: zrk@ustc.edu

magnetization and Curie temperature,[16,24] the effects of the in-plane strain on EPS, the way the lattice strain interacts with magnetic field, how the relative strength of EPS evolves with lattice strain, magnetic field, and temperature. There is no doubt that a systematic experimental investigation of the effects of domain switching on the lattice strain, electronic transport, and magnetic properties is highly needed in order to obtain a more in-depth understanding of the lattice strain effect and interfacial charge effect of $La_{1-x}Ba_xMnO_3$/FE crystal heterostructures, which is undoubtedly also important for realizing non-volatile memory applications of this class of materials.

In this paper, we have utilized (001)-, (110)-, and (111)-oriented $0.31Pb(In_{1/2}Nb_{1/2})O_3$-$0.35Pb(Mg_{1/3}Nb_{1/2})O_3$-$0.34PbTiO_3$ (PINT) ferroelectric single-crystal substrates to grow $La_{0.8}Ba_{0.2}MnO_3$ (LBM020) and $La_{0.6}Ba_{0.4}MnO_3$ (LBM040) epitaxial films and *in situ* modulated the in-plane tensile strain of the films by appropriately controlling the ferroelectric domain switching of the PINT substrates. Our study mainly focuses on investigating the effects of domain-switching-induced strain and electric charge on the electronic transport and magnetic properties of the films, the evolution of the strength of EPS against temperature, lattice strain, and magnetic field, the interaction between the lattice strain and the magnetic field, and the reversible and non-volatile resistance switching of the films using the ferroelastic domain switching of the PINT substrates.

II. EXPERIMENTAL DETAILS

A PINT single-crystal boule with a size of $\Phi 50 \times 70\,mm^3$ was grown by a modified Bridgman technique at the Shanghai Institute of Ceramics. The crystal growth details were described in Ref. 25. The as-grown PINT crystal boule was cut into (001)-, (110)-, and (111)-oriented rectangular plates ($10 \times 5 \times 0.5\,mm^3$) and carefully polished to a surface root-mean-square roughness $R_q < 1$ nm. LBM020 and LBM040 films were grown on the (001)-, (110)-, and (111)-oriented PINT(111) substrates by the pulsed laser deposition at a substrate temperature of 700 °C and an oxygen pressure of 27 Pa. After deposition, the films were immediately *in situ* annealed at 1×10^5 Pa oxygen for 60 min to reduce oxygen deficiency then cooled to room temperature at 5 °C/min. The laser energy density and the repetition rate were $3\,J/cm^2$ and 5 Hz, respectively. The thickness of the films was estimated to be ~40 nm, as illustrated by the cross-sectional back-scattered electron (BSE) image shown in Fig. 1(f). Atomic force microscopy (AFM) measurements show that all films have a smooth surface with $R_q \sim 1.3$ nm.

The local ferroelectric responses of the PINT substrates were characterized by means of piezoresponse force microscopy (PFM), using a Dimension V (VEECO) microscope with conducting tip and no top electrode. The phase purity of the films and the epitaxial relationships between the films and the substrates were characterized by the out-of-plane and in-plane θ-2θ linear scans and phi scans, respectively, using a high resolution Bruker D8 Discover (Cu $K_{\alpha 1}$ radiation, $\lambda = 1.5406$ Å) x-ray diffractometer (XRD) equipped with 4-bounce Ge(220) monochromator. Fig. 1(c) shows a schematic of the experimental setup for *in situ* measurements of electric-field-induced out-of-plane strain of the PINT substrate [$\delta\varepsilon_{zz(PINT)}$] and the LBM020 (LBM040) film [$\delta\varepsilon_{zz(Film)}$] using XRD θ–2θ scans. Here, $\delta\varepsilon_{zz}$ was calculated using the equation $\delta\varepsilon_{zz} = [c(E) - c(0)]/c(0)$, where $c(E)$ and $c(0)$ are the lattice constant c of the PINT substrate or the LBM020 (LBM040) film when an electric field E or a zero E was applied across the PINT substrate. The electric-field-induced in-plane strain in the PINT substrate (i.e., $\delta\varepsilon_{xx(PINT)}$) was measured by a strain gauge that was attached onto the substrate surface with epoxy [see Fig. 1(e)]. The ferroelectric poling along the [001], [110], or [111] crystal direction and the 180° and non-180° domain switching were achieved by applying an appropriate *dc* electric field across the PINT substrate through the conducting LBM020 (LBM040) film and the sputtered bottom Au electrode using a Keithley 6517B electrometer. The resistance of the LBM020 and LBM040 films was measured with the physical property measurement system (PPMS-9, Quantum Design), using the standard four probe method employing the experimental setup shown in Fig. 1(d). Magnetic data were collected using a SQUID magnetometer (MPMS XL-5, Quantum Design) with the magnetic field applied parallel to the film plane.

III. RESULTS AND DISCUSSION

The XRD θ-2θ scan pattern for the LBM020/PINT(111) structure shown in Fig. 1(a) suggests that the LBM020 film has no impurities and is highly (111)-oriented. The in-plane orientation of the film with respect to that of the substrate was assessed by examining XRD ϕ-scans that were taken on the (101) diffraction peaks of the LBM020 film and the PINT substrate, respectively. As presented in the inset of Fig. 1(a), the diffraction peaks of the film occur at the same azimuthal ϕ angle as those of the PINT substrate and are 120° apart from each other. This clearly indicates the presence of three-fold symmetry along the (111) direction and epitaxial growth of the LBM020 film on the PINT substrate. A schematic of the in-plane lattice arrangements for the LBM020 film on the PINT substrate is shown in Fig. S1 of the supplementary material.[26] Note that similar XRD θ-2θ and ϕ scan patterns have been found for the LBM040 film grown on the PINT(111) substrate [see Fig. 1(b)]. The out-of-plane lattice spacing d_{111} (~2.252 Å) of the LBM040 film calculated from the LBM040 (111) diffraction peak is smaller than that of the LBM040 bulk value (~2.263 Å) obtained by Rietveld refinement from all diffraction peaks of the LBM040 bulk, revealing that the LBM040 film is subjected to an in-plane tensile strain and an out-of-plane compressive strain (−0.49%). This is in accordance with the fact that the lattice parameters ($a \sim b \sim c \sim 3.92$ Å) of the LBM040 bulk are smaller than those ($a \sim b \sim c \sim 4.02$ Å) of the PINT substrate.

Fig. 2 illustrates the temperature dependence of the resistance under magnetic fields for the LBM020 film when the PINT(111) substrate was in the unpoled P_r^0 and positively poled P_r^+ states (i.e., electric dipole moments point to the LBM020 film), respectively. For the P_r^0 state and $H = 0$ T, upon decreasing temperature, the LBM020 film undergoes an insulator-to-metal phase transition near $T_C \sim 238$ K when the FMM phase and the paramagnetic insulating (PMI) phase

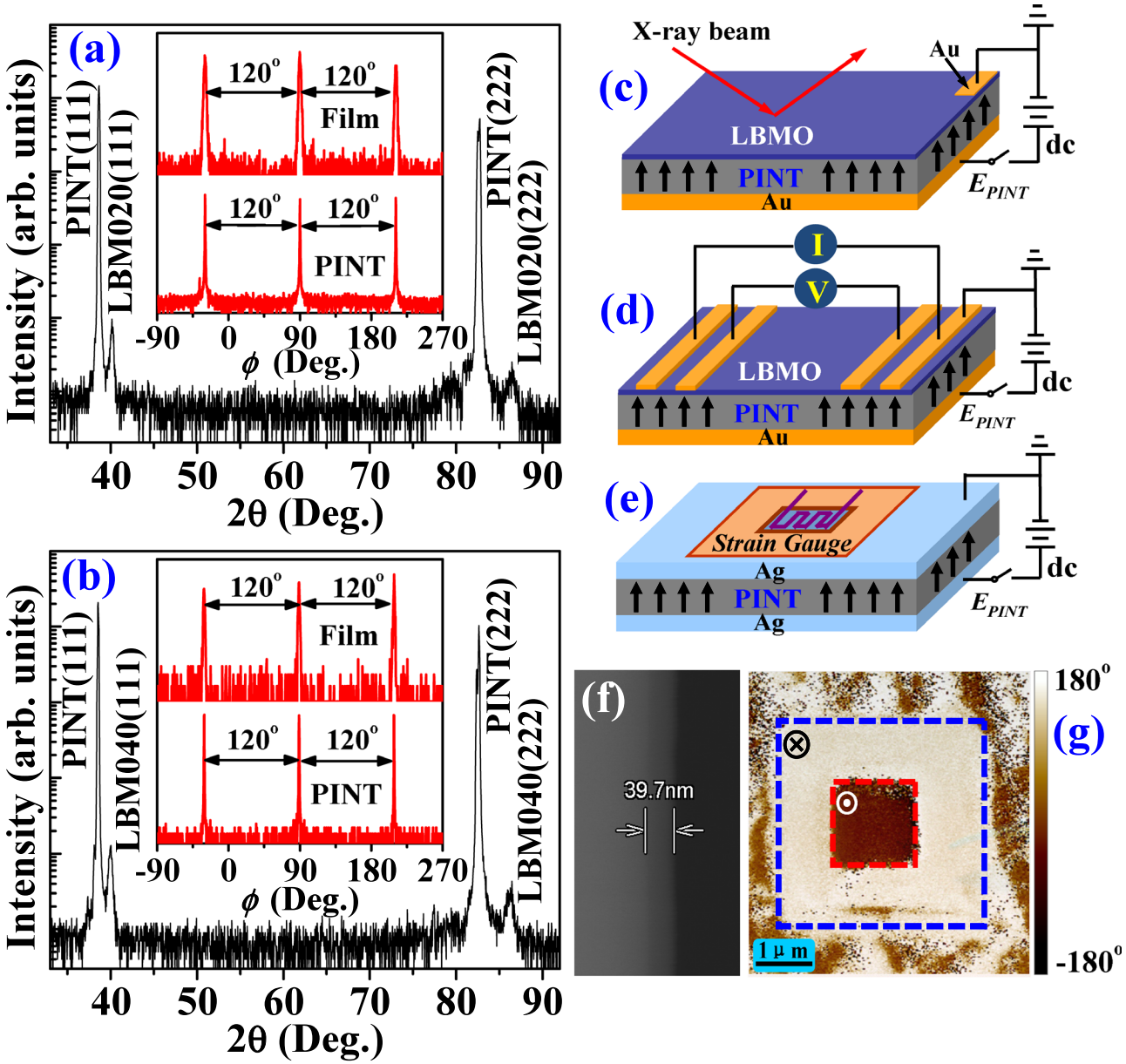

FIG. 1. XRD θ-2θ scans of the $La_{0.8}Ba_{0.2}MnO_3$ (a) and $La_{0.6}Ba_{0.4}MnO_3$ (b) films. Insets: Corresponding XRD ϕ scans taken on the film (101) and PINT (101) diffraction peaks. (c), (d), and (e) show schematic of the experimental setups for *in situ* measurements of film strain, resistance, and in-plane strain of the PINT substrate, respectively. (f) and (g) show the cross-sectional BSE image of the $La_{0.6}Ba_{0.4}MnO_3$ film and the out-of-plane PFM image of the PINT(111) substrate, respectively.

coexist and strongly compete with each other,[27,28] and re-enters into the charge-ordered insulating (COI) state near $T_{CO} \sim 164$ K where the resistance shows an upturn. The electronic conducting behavior over the whole temperature range is quite similar to that of the lightly doped $La_{1-x}Ca_xMnO_3$ ($x = 0.15$, 0.2)[29] and $La_{1-x}Sr_xMnO_3$ ($0.11 \leq x \leq 0.13$)[30] bulk materials in which the charge-ordered phase appears at low temperatures. *In situ* XRD θ-2θ scans near the PINT(111) and LBM020(111) diffraction peaks under the application of an electric field to the PINT substrate (not shown here) revealed that the poling-induced $\delta\varepsilon_{xx(PINT)}$, which is perpendicular to the [111] crystal direction, was transferred to the LBM020 film through strain coupling across the interface. As a consequence, the in-plane tensile strain of the LBM020 film is reduced significantly, which leads to the conversion of a portion of the PMI and COI phases into the FMM phase, as manifested by the poling-induced significant reduction in the resistance and T_{CO} and considerable enhancement of T_C. Another noteworthy feature is that, regardless of whether the PINT(111) substrate was in the P_r^0 or P_r^+ state, T_{CO} and T_C of the LBM020 film increase with increasing H, which is similar to that observed in the $La_{7/8}Sr_{1/8}MnO_3$ single crystals.[31] The similarity in the magnetic-field-induced enhancement of both T_{CO} and T_C in the LBM020 film and the charge-ordered $La_{7/8}Sr_{1/8}MnO_3$ single crystals further reveals that the upturn of the resistance near $T = 164$ K for the P_r^0 state and $T = 161$ K for the P_r^+ state in the LBM020 film is due to the charge ordering.

To gain insight into the correlation between the poling-induced strain and the EPS, we measured the strain-tunability

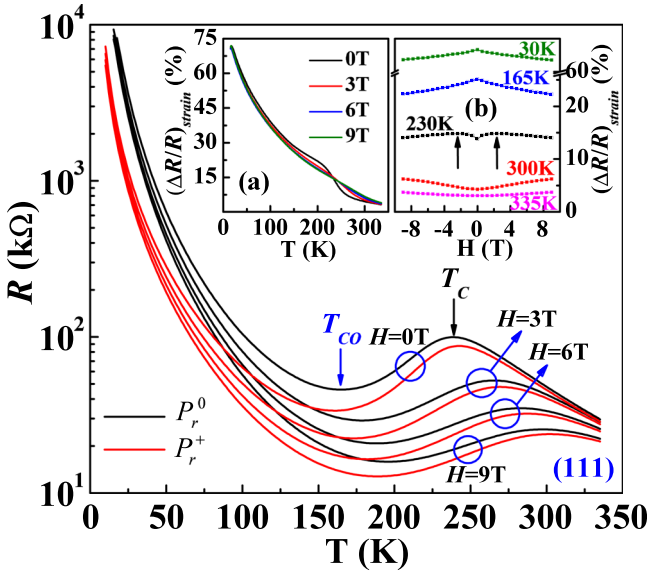

FIG. 2. Temperature dependence of the resistance for the $La_{0.8}Ba_{0.2}MnO_3$ film under $H = 0$, 3, 6, and 9 T when the PINT(111) substrate was in the P_r^0 and P_r^+ states, respectively. Inset (a) shows temperature dependence of $(\Delta R/R)_{strain}$ under $H = 0$, 3, 6, and 9 T for the $La_{0.8}Ba_{0.2}MnO_3$ film. Inset (b) shows $(\Delta R/R)_{strain}$ versus H for the $La_{0.8}Ba_{0.2}MnO_3$ film at temperatures as stated.

of the resistance $(\Delta R/R)_{strain}$ $[(\Delta R/R)_{strain} = [R(P_r^0) - R(P_r^+)]/R(P_r^0)]$ as a function of temperature and showed the results in the inset (a) of Fig. 2. For $H = 0$ T, $(\Delta R/R)_{strain}$ increases with decreasing temperature and reaches a maximal value of 71.8% at $T = 17$ K, indicating quite sensitive of the COI phase to the lattice strain at low temperatures. Apparently, $(\Delta R/R)_{strain}$ is dependent of the magnetic field which considerably enhances $(\Delta R/R)_{strain}$ in high temperature region (above T_C), but suppresses it in low temperature region (below T_C), showing opposing effects of the magnetic field on the strain effect. For example, $(\Delta R/R)_{strain}$ at $T = 267$ K (higher than T_C) is increased from 6.7% for $H = 0$ T to 10.5% for $H = 9$ T, an enhancement of approximately 57%, while $(\Delta R/R)_{strain}$ at $T = 200$ K (lower than T_C) is reduced from 22.1% for $H = 0$ T to 18.5% for $H = 9$ T. All the above data clearly demonstrate the strong coupling between the lattice strain and the magnetic field, which is mediated by the EPS.

To further explore the evolution of the relative strength of the EPS with magnetic field, $(\Delta R/R)_{strain}$ was plotted against H, as depicted in the inset (b) of Fig. 2. The isothermal $(\Delta R/R)_{strain}$ increases monotonously with increasing H for $T > T_C$ (e.g., $T = 300$ and 335 K) but decreases with increasing H for $T < T_C$ (e.g., $T = 30$ and 165 K), revealing that the strength of EPS is enhanced by H for $T > T_C$ but suppressed by H for $T < T_C$. However, at around T_C, e.g., $T = 230$ K, $(\Delta R/R)_{strain}$ initially increases with increasing H and reaches the maximum value at $H = 2.4$ T, then drops with further increase in H. This evolution of $(\Delta R/R)_{strain}$ against H demonstrates that the strength of the EPS is the strongest at $H = 2.4$ T and suppressed when H deviates (either increase or decrease) from $H = 2.4$ T. For $H < 2.4$ T, the PMI phase dominates over the FMM phase, while for $H > 2.4$ T, the latter dominates over the former. Around $H = 2.4$ T, the coexisting two phases strongly compete with each other and shows the maximal EPS tendency with the minimum energy difference between the coexisting FMM and PMI phases. A small external perturbation (e.g., the poling-induced strain) could easily covert the PMI phase to the FMM phase, causing a decrease in the resistance. Note that similar effects of poling-induced strain on the resistance and magnetic field on the $(\Delta R/R)_{strain}$ have also been found for the LBM020 films grown on the (001)- and (110)-oriented PINT substrates (see Fig. S2 of the supplementary material[26]). These findings demonstrate the effectiveness of magnetic-field modulation of the strain effect, which can be understood within the framework of the EPS.

For the LBM040 film, as can be seen in Fig. S3 of the supplementary material,[26] the overall conducting behavior throughout the whole temperature range and the impact of poling-induced strain on the resistance are similar to a previous report on $La_{0.67}Ba_{0.33}MnO_3$ films by Zhu *et al.*[19] It is noteworthy that, if a negative reverse electric field of $E = -8$ kV/cm was applied to the positively poled PINT substrate along the [-1–1-1] direction at $T = 296$ K, the resistance of the LBM040 film undergoes a peak near $E = -3.5$ kV/cm then followed by a sharp drop upon further increase in E [inset (a) of Fig. S3]. Such dramatic resistance change near E_C of the PINT substrate is apparently associated with the 180° ferroelectric domain switching, which would induce a large in-plane tensile strain during the domain switching process.[10,21,22] After the PINT substrate had been switched to the P_r^- state (i.e., electric dipole moments point to the bottom Au electrode), we turned off the external *dc* electric field and found that the resistance returns to its initial value at $E = 0$ kV/cm. Moreover, whether the film is under $H = 0$, 3, 6, or 9 T, the resistance for the P_r^+ state is similar to that for the P_r^- state over the entire temperature range [inset (b) of Fig. S3]. All these results establish that the 180° ferroelectric domain switching-induced accumulation/depletion of charge carriers at the interface has little impact on the electronic transport properties of the LBM040/PINT structure, implying strain but not polarity induced nature of the resistance change. We note that PFM measurements on an unpoled PINT substrate demonstrate that the poling-induced strain microscopically originates from the rotation of ferroelectric domains towards the out-of-plane direction upon poling along the [111] direction, as can be seen in Fig. 1(g), where sharp contrast appears upon poling.

The ferroelectric poling-induced strain does not only significantly affect the resistance but also considerably influence the magnetic properties of the LBM020 and LBM040 films. Fig. 3 shows the temperature dependence of the zero-field-cooled (ZFC) and field-cooled (FC) magnetization (M) of the LBM040/PINT(111) structure when the PINT substrate was in the P_r^0 and P_r^+ states, respectively. A pronounced intersection in the ZFC (or FC) M versus T curve appears near $T \sim 150$ K between the P_r^0 and P_r^+ states, indicative of opposing effects of the poling-induced strain on M. For $T > 150$ K, T_C is enhanced after poling, resulting in an increase in M. In contrast, M is reduced remarkably by the poling-induced in-plane compressive strain for $T < 150$ K. The relative change in the magnetization $(\Delta M/M)$ for ZFC, $\Delta M/M = [M(P_r^0) - M(P_r^+)]/M(P_r^0)$, reaches 14% at

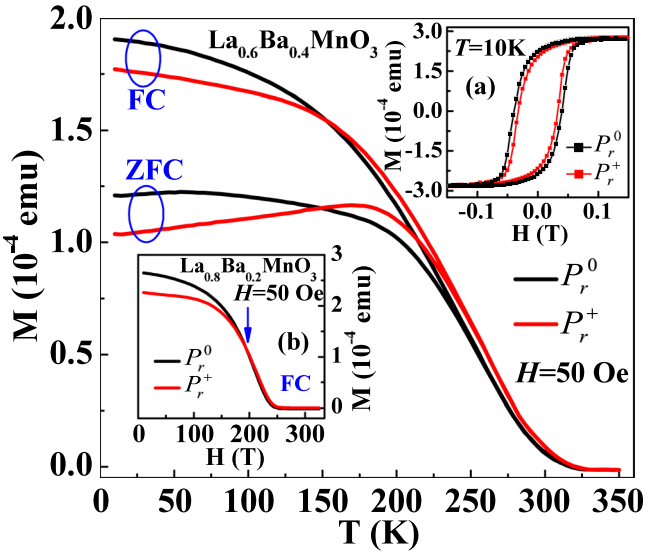

FIG. 3. Temperature dependence of ZFC and FC magnetization (M) for the $La_{0.6}Ba_{0.4}MnO_3$ film when the PINT(111) substrate was in the P_r^0 and P_r^+ states, respectively. Inset (a) shows the magnetic hysteresis curves at $T = 10$ K for the $La_{0.6}Ba_{0.4}MnO_3$ film when the PINT(111) substrate was in the P_r^0 and P_r^+ states, respectively. Inset (b) shows M versus T curve for the $La_{0.8}Ba_{0.2}MnO_3$ film when the PINT(111) substrate was in the P_r^0 and P_r^+ states, respectively.

$T = 10$ K for $H = 50$ Oe. This value is consistent with the poling-induced decrease in the remnant M at $T = 10$ K, accompanied by a concurrent change in magnetic anisotropy,[32] as deduced from the magnetic hysteresis loops shown in the inset (a) of Fig. 3. The poling-induced strain not merely changes the Mn-O bond lengths and Mn-O-Mn bond angles but also induces a magnetoelastic anisotropy energy (K_{me}) in the film plane via the inverse magnetostriction.[33]

Here, $K_{me} = \frac{3}{2}\lambda\sigma$[33,34] where λ is the in-plane magnetostriction coefficient whose value evolves from negative to positive with decreasing temperature for manganites[35] and σ is the induced in-plane stress. The magnetoelastic energy could lead to a uniaxial anisotropy and the stress anisotropy energy reads $E_{me} = K_{me}\sin^2\theta$,[33,34] where θ is the angle between M and the σ-axis. At high temperatures ($T > 150$ K), λ is negative, σ is positive under tensile stress and hence $K_{me} < 0$, which favors $\theta = \pi/2$, i.e., perpendicular alignment of M relative to the stress axis in the film plane. Upon poling, the in-plane tensile strain is partly released, reducing the in-plane K_{me} and thus causing an increase in M. At low temperatures ($T < 150$ K), λ becomes positive[35] and thus $K_{me} > 0$, favoring parallel alignment of M with $\theta = 0$. The poling-induced release of the tensile strain in the film also reduces the K_{me}, giving rise to less parallel alignment of M and thus smaller in-plane M along the magnetic field direction. Based on this, it is understandable that the opposing effects of poling-induced strain on the magnetic properties are a consequence of strain-induced magnetic anisotropy via the magnetoelastic effect. It is noted that similar results have been found for the LBM020/PINT(111) structure [inset (b) of Fig. 3].

To substantiate the strain effects in the LBM040/PINT(111) structure, we *in situ* reversibly modulated the resistance of the LBM040 film using the ferroelastic domain switching of the PINT substrate. Figs. 4(d) and 4(e) show the $\Delta R/R$ of the LBM040 film and the in-plane strain $\varepsilon_{xx(PINT)}$ of the PINT substrate as a function of E, respectively. Upon applying a sufficient large bipolar E [$E > E_{C(PINT)}$] across the substrate, a butterfly-like $\varepsilon_{xx(PINT)}$–E curve (red) [Fig. 4(e)] was found, stemming from the 180° ferroelectric domain switching. However, non-180° domain switching was

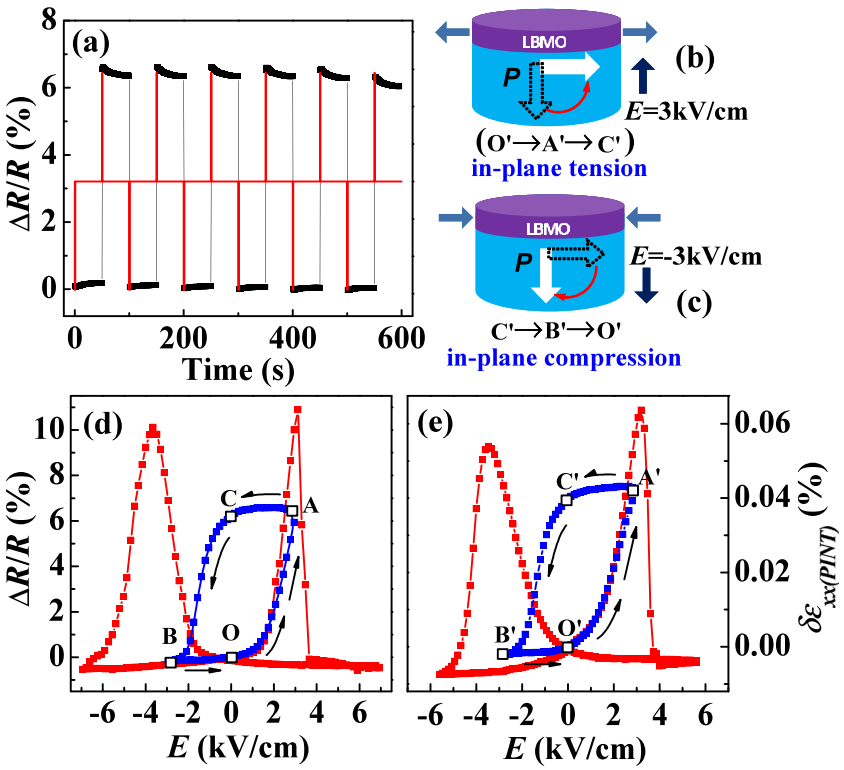

FIG. 4. (a) Non-volatile resistance switching of the $La_{0.6}Ba_{0.4}MnO_3$ film by a pulse electric field at $T = 296$ K. (b) and (c) show schematic diagrams for the ferroelastic domain switching. (d) and (e) show electric-field-induced $\Delta R/R$ of the $La_{0.6}Ba_{0.4}MnO_3$ film and the in-plane strain of the PINT(111) substrate as a function of bipolar and unipolar E applied across the PINT(111), respectively.

induced if an appropriate unipolar E [$E < E_{C(PINT)}$] was applied across the PINT substrate,[10,20–22] resulting in a hysteretic $\varepsilon_{xx(PINT)}$–E loop (blue) with a remnant strain. Regardless of whether a bipolar or a unipolar E was applied, the electric-field-induced resistance modulation $\Delta R/R$ strongly depends on the induced $\varepsilon_{xx(PINT)}$. As can be seen in Fig. 4(d), $\Delta R/R$ versus E curve exhibits a typical butterfly-like shape (red) for $E > E_{C(PINT)}$, while a hysteretic loop-like $\Delta R/R \sim E$ curve (blue) was found for $E < E_{C(PINT)}$, indicating that it is the strain transferred from the PINT substrate that determines the changes of the resistance. This hysteretic resistance behavior can be qualitatively explained using the schematic diagrams shown in Figs. 4(b) and 4(c). With the application of a positive $E = +3$ kV/cm (lower than $E_{C(PINT)}$) to the negatively poled PINT substrate, 71° and/or 109° ferroelastic domain switching was induced, resulting in the rotation of the polarization vectors from the downward direction towards the in-plane direction [Fig. 4(b)].[10,20–22] Consequently, an in-plane tensile strain was induced in the PINT substrate, corresponding to the evolution of $\varepsilon_{xx(PINT)}$ from $\mathbf{O}'$ to $\mathbf{A}'$. Once the electric field is removed, the in-plane strain mainly remains, namely, $\varepsilon_{xx(PINT)}$ changes from $\mathbf{A}'$ to $\mathbf{C}'$ but not return to $\mathbf{O}'$. The film resistance is retained (from **A** to **C** not to **O**), due to the stability of the remnant in-plane polarization in the PINT.[10,20–23] Afterwards, the in-plane polarization vectors were switched from the in-plane direction back to the downward direction from $\mathbf{C}'$ to $\mathbf{B}'$ through applying a negative E of -3 kV/cm to the PINT substrate, removing the previously induced remnant strain. After the $E = -3$ kV/cm electric field was turned off, the in-plane strain recovers to $\mathbf{O}'$ state. The film resistance thus returns to the initial value (i.e., **O** state). Consequently, these two distinct stable, switchable, and non-volatile ferroelastic strain states ($\mathbf{O}'$ and $\mathbf{C}'$) yield two stable, reversible, and non-volatile resistance states (**O** and **C**). As can be seen in Fig. 4(a), non-volatile resistance modulation of the LBM040 film can be achieved by applying a pulse *dc* electric field of $E = \pm 3$ kV/cm across the PINT substrate to switch the polarization vectors between the in-plane and downward directions. A resistance modulation up to ~6.5% was achieved at room temperature, which is superior to other reports.[5,21] The electric-field-tuned non-volatile and reversible resistance switching via the ferroelastic effect could have potential applications for non-volatile memory devices.

IV. CONCLUSIONS

In summary, LBM020 and LBM040 films have been epitaxially grown on (001)-, (110)-, and (111)-oriented PINT ferroelectric substrates. The 180° domain switching has little effects on the electronic transport properties of the LBM040 film in the whole temperature region, demonstrating that it is the poling-induced strain but not the poling-induced electrostatic charge that mediates the electric-field-control of the electronic and magnetic properties of the films. Ferroelectric poling along the [001], [110], or [111] direction causes partly melting of the PMI and CO phases associated with a considerable enhancement in T_C and a drop in T_{CO} and resistance by 71.8%. Opposing effects of magnetic field on the strain-tunability of resistance [$(\Delta R/R)_{strain}$] were found above and below the Curie temperature T_C, which is closely associated with the electronic phase separation whose relative strength can be determined by measuring $(\Delta R/R)_{strain}$ as a function of magnetic field. Furthermore, it was found that the poling-induced strain has an opposing effect on the ferromagnetism of the LBM040 (LBM020) film above and below 150 K (197 K), which can be understood in terms of the magnetoelastic coupling that tunes the magnetic anisotropy of the film. Finally, we realized non-volatile and reversible resistance switching in the LBM040/PINT(111) structure at room temperature using the ferroelastic effect of the PINT substrate, which may have potential applications in non-volatile memory devices.

ACKNOWLEDGMENTS

This work was supported by the National Natural Science Foundation of China (Grant Nos. 51172259 and 11090332) and the CAS/SAFEA International Partnership Program for Creative Research Teams.

[1]R. O. Cherifi, V. Ivanovskaya, L. C. Phillips, A. Zobelli, I. C. Infante, E. Jacquet, V. Garcia, S. Fusil, P. R. Briddon, N. Guiblin, A. Mougin, A. A. Ünal, F. Kronast, S. Valencia, B. Dkhil, A. Barthélémy, and M. Bibes, Nature Mater. **13**, 345 (2014).
[2]Z. G. Wang, Y. Zhang, R. Viswan, Y. X. Li, H. S. Luo, J. F. Li, and D. Viehland, Phys. Rev. B **89**, 035118 (2014).
[3]J. F. Wang, Y. C. Jiang, Z. P. Wu, and J. Gao, J. Appl. Phys. **113**, 17D911 (2013).
[4]M. Liu, Z. Y. Zhou, T. X. Nan, B. M. Howe, G. J. Brown, and N. X. Sun, Adv. Mater. **25**, 1435 (2013).
[5]Y. J. Yang, Z. L. Luo, M. M. Yang, H. L. Huang, H. B. Wang, J. Bao, G. Q. Pan, C. Gao, Q. Hao, S. T. Wang, M. Jokubaitis, W. Z. Zhang, G. Xiao, Y. P. Yao, Y. K. Liu, and X. G. Li, Appl. Phys. Lett. **102**, 033501 (2013).
[6]M. C. Dekker, A. D. Rata, K. Boldyreva, S. Oswald, L. Schultz, and K. Dörr, Phys. Rev. B **80**, 144402 (2009).
[7]Q. P. Chen, J. J. Yang, Y. G. Zhao, S. Zhang, J. W. Wang, M. H. Zhu, Y. Yu, X. Z. Zhang, Z. Wang, B. Yang, D. Xie, and T. L. Ren, Appl. Phys. Lett. **98**, 172507 (2011).
[8]J. Wang, J. M. Hu, H. Wang, H. Jiang, Z. B. Wu, J. Ma, X. H. Wang, Y. H. Lin, and C. W. Nan, J. Appl. Phys. **107**, 083901 (2010).
[9]R. K. Zheng, Y. Wang, H. L. W. Chan, C. L. Choy, and H. S. Luo, Appl. Phys. Lett. **90**, 152904 (2007).
[10]T. Wu, A. Bur, P. Zhao, K. P. Mohanchandra, K. Wong, K. L. Wang, C. S. Lynch, and G. P. Carman, Appl. Phys. Lett. **98**, 012504 (2011).
[11]H. Lu, T. A. George, Y. Wang, I. Ketsman, J. D. Burton, C. W. Bark, S. Ryu, D. J. Kim, J. Wang, C. Binek, P. A. Dowben, A. Sokolov, C. B. Eom, E. Y. Tsymbal, and A. Gruverman, Appl. Phys. Lett. **100**, 232904 (2012).
[12]H. J. A. Molegraaf, J. Hoffman, C. A. F. Vaz, S. Gariglio, D. van der Marel, C. H. Ahn, and J.-M. Triscone, Adv. Mater. **21**, 3470 (2009).
[13]C. A. F. Vaz, J. Hoffman, Y. Segal, J. W. Reiner, R. D. Grober, Z. Zhang, C. H. Ahn, and F. J. Walker, Phys. Rev. Lett. **104**, 127202 (2010).
[14]P. M. Leufke, R. Kruk, R. A. Brand, and H. Hahn, Phys. Rev. B **87**, 094416 (2013).
[15]T. X. Nan, Z. Y. Zhou, M. Liu, X. Yang, Y. Gao, B. A. Assaf, H. Lin, S. Velu, X. J. Wang, H. S. Luo, J. Chen, S. Akhtar, E. Hu, R. Rajiv, K. Krishnan, S. Sreedhar, D. Heiman, B. M. Howe, G. J. Brown, and N. X. Sun, Sci. Rep. **4**, 3688 (2014).
[16]J. Zhang, H. Tanaka, T. Kanki, J. H. Choi, and T. Kawai, Phys. Rev. B **64**, 184404 (2001).
[17]T. Kanki and Y. G. Park, Appl. Phys. Lett. **83**, 4860 (2003).
[18]X. Y. Li, M. Zheng, Q. X. Zhu, M. M. Yang, X. M. Li, X. Shi, G. L. Yuan, Y. Wang, H. L. W. Chan, X. G. Li, H. S. Luo, and R. K. Zheng, Mater. Chem. Phys. **144**, 470 (2014).
[19]Q. X. Zhu, M. Zheng, M. M. Yang, X. M. Li, Y. Wang, X. Shi, H. L. W. Chan, H. S. Luo, X. G. Li, and R. K. Zheng, Appl. Phys. Lett. **103**, 132910 (2013).
[20]M. M. Yang, X. Q. Zhao, J. Wang, Q. X. Zhu, J. X. Zhang, X. M. Li, H. S. Luo, X. G. Li, and R. K. Zheng, Appl. Phys. Lett. **104**, 052902 (2014).

[21]M. Liu, J. Hoffman, J. Wang, J. X. Zhang, B. Nelson-Cheeseman, and A. Bhattacharya, Sci. Rep. **3**, 1876 (2013).
[22]B. W. Zhi, G. Y. Gao, H. R. Xu, F. Chen, X. L. Tan, P. F. Chen, L. F. Wang, and W. B. Wu, ACS Appl. Mater. Interfaces **6**, 4603 (2014).
[23]S. Zhang, Y. G. Zhao, P. S. Li, J. J. Yang, S. Rizwan, J. X. Zhang, J. Seidel, T. L. Qu, Y. J. Yang, Z. L. Luo, Q. He, T. Zou, Q. P. Chen, J. W. Wang, L. F. Yang, Y. Sun, Y. Z. Wu, X. Xiao, X. F. Jin, J. Huang, C. Gao, X. F. Han, and R. Ramesh, Phys. Rev. Lett. **108**, 137203 (2012).
[24]Q. S. Yuan, Phys. Rev. B **70**, 066401 (2004).
[25]Y. Y. Zhang, X. B. Li, D. A. Liu, Q. H. Zhang, W. Wang, B. Ren, D. Lin, X. Y. Zhao, and H. S. Luo, J. Cryst. Growth **318**, 890 (2011).
[26]See supplementary material at http://dx.doi.org/10.1063/1.4896172 for Figs. S1, S2, and S3.
[27]T. Z. Ward, J. D. Budai, Z. Gai, J. Z. Tischler, L. F. Yin, and J. Shen, Nat. Phys. **5**, 885 (2009).
[28]H. W. Guo, J. H. Noh, S. Dong, P. D. Rack, Z. Gai, X. S. Xu, E. Dagotto, J. Shen, and T. Z. Ward, Nano Lett. **13**, 3749 (2013).
[29]G.-L. Liu, J.-S. Zhou, and J. B. Goodenough, Phys. Rev. B **70**, 224421 (2004).
[30]B. Dabrowski, X. Xiong, Z. Bukowski, R. Dybzinski, P. W. Klamut, J. E. Siewenie, O. Chmaissem, J. Shaffer, C. W. Kimball, J. D. Jorgensen, and S. Short, Phys. Rev. B **60**, 7006 (1999).
[31]S. Uhlenbruck, R. Teipen, R. Klingeler, B. Büchner, O. Friedt, M. Hücker, H. Kierspel, T. Niemöller, L. Pinsard, A. Revcolevschi, and R. Gross, Phys. Rev. Lett. **82**, 185 (1999).
[32]J. Y. Kim, L. Yao, and S. Van Dijken, J. Phys.: Condens. Matter **25**, 082205 (2013).
[33]S. Sahoo, S. Polisetty, C.-G. Duan, S. S. Jaswal, E. Y. Tsymbal, and C. Binek, Phys. Rev. B **76**, 092108 (2007).
[34]J. W. Wang, Y. G. Zhao, C. Fan, X. F. Sun, S. Rizwan, S. Zhang, P. S. Li, Z. Lin, Y. J. Yang, W. S. Yan, Z. L. Luo, L. K. Zou, H. L. Liu, Q. P. Chen, X. Zhang, M. H. Zhu, H. Y. Zhang, J. W. Cai, X. F. Han, Z. H. Cheng, C. Gao, D. Xie, and T. L. Ren, Appl. Phys. Lett. **102**, 102906 (2013).
[35]L. I. Koroleva, R. V. Demin, A. V. Kozlov, D. M. Zashcherinskii, O. Y. Gorbenko, A. R. Kaul, O. V. Melnikov, and Y. M. Mukovskii, J. Magn. Magn. Mater. **316**, E644 (2007).